

Collision between chemically-driven self-propelled drops

Shunsuke Yabunaka¹†, and Natsuhiko Yoshinaga²‡,

¹Yukawa Institute for Theoretical Physics, The Kyoto University, Kitashirakawa Oiwake-Cho, 606-8502 Kyoto, Japan

²WPI - Advanced Institute for Materials Research, Tohoku University, Sendai 980-8577, Japan

(Received xx; revised xx; accepted xx)

We consider analytically and numerically head-on collision between two self-propelled drops. Each drop is driven by chemical reactions that produce or consume the concentration isotropically. The isotropic distribution of the concentration field is destabilized by motion of the drop which is itself made by Marangoni flow from concentration-dependent surface tension. This symmetry-breaking self-propulsion is distinct from other self-propulsion mechanisms due to the intrinsic polarity such as squirmers and self-phoretic motion; there is a bifurcation point below which the drop is stationary and above which it moves spontaneously. When two drops moving along the same axis with opposite direction, the interactions arise both from hydrodynamics and concentration overlap. We found that two drops exhibit either elastic collision or fusion depending on the distance from the bifurcation point controlled, for instance, by viscosity. The elastic collision results from the balance between dissipation and energy injection by chemical reactions. We derive the reduced equations for the collision between two drops and analyze the contributions from the two interactions. The concentration-mediated interaction is found to dominate the hydrodynamic interaction.

1. Introduction

In biological systems, cells and microorganisms are moving spontaneously and autonomously by consuming energy from ATP hydrolysis. The size and swimming speed of a bacteria are small so that self-propulsion is described by the low-Reynolds-number hydrodynamics. In order to capture the generic mechanism of the self-propulsion, several mathematical models have been investigated. Among them, The squirmer model focuses on the flow field created by beating of cilia on a body of a microorganism and/or deforming the body surface itself (Lighthill 1952; Blake 1971). The problem then falls in solving the Stokes equation with boundary conditions with finite velocity on the body in the normal and/or tangential directions. The motion of the single squirmer, the translational and angular velocities, are well understood (Stone & Samuel 1996). Apart from the model, there have been several attempts to find other classes of self-propulsion. The minimal extension of the model is to include an additional scalar field such as a concentration, electric, or temperature field. An asymmetric particle with two different surface properties, which is called a Janus particle, generates a gradient of the field around the particle and spontaneously moves (Paxton *et al.* 2004; Howse *et al.* 2007; Jiang *et al.* 2010). The motion is similar to phoresis but the gradient is self-generated instead of being imposed. This mechanism is thus called self-phoresis.

† Email address for correspondence: yabunaka@scphys.kyoto-u.ac.jp

‡ Email address for correspondence: yoshinaga@wpi-aimr.tohoku.ac.jp

The squirmer and Janus particles have intrinsic asymmetry and therefore the swimming direction is set by the polar direction of the asymmetry on the particle itself. This makes the problem simpler; there is a linear relation between the self-propulsion speed and the magnitude of the asymmetry. On the other hand, cells often break the symmetry to choose the direction of motion (Yam *et al.* 2007). This phenomenon is not captured by the squirmer and Janus particles, and therefore another class of self-propulsion has to be considered. Toward this direction, several mathematical models that include the internal polarity field have been proposed (Shao *et al.* 2010; Ziebert *et al.* 2012; Tjhung *et al.* 2012). In these models, indeed the spontaneous symmetry breaking was observed to reproduce the directional motion.

Along this line, it was recently found that non-living chemically-driven systems exhibit self-propulsion (Toyota *et al.* 2009; Thutupalli *et al.* 2011; Izri *et al.* 2014). In these systems, the drop may produce or consume chemical molecules so that the systems are away from equilibrium states. The flux couples with the motion and results in asymmetric concentration distribution. Once the symmetry is broken, the surface tension becomes anisotropic and creates flow inside and outside the drop. The motion under a given gradient of concentration and/or temperature fields is known as the Marangoni effect (Young *et al.* 1959; Fedosov 1956). The self-propulsive motion using the Marangoni effect under the chemical reaction was first proposed as *a reactive drop* in (Ryazantsev 1985) and theoretically reformulated as bifurcation phenomena (Yabunaka *et al.* 2012; Yoshinaga *et al.* 2012; Yoshinaga 2014). In these works, the reduced nonlinear equations are derived from the coupled advection-diffusion and hydrodynamic equations. The similar idea has then been discussed for the auto-phoretic motion, where the self-phoretic motion exemplified by the Janus particle is realized due to *isotropic* chemical reaction coupled with advection in a nonlinear fashion (Michelin *et al.* 2013).

In contrast with the self-propulsion of a isolated particle/drop, understandings of the interaction between them is still limited. For the squirmer, there have been intensive numerical studies of interaction between squirmers (Ishikawa *et al.* 2006) and the interaction between the squirmer and the wall (Spagnolie & Lauga 2012). In particular, the understanding of the squirmer/wall system has recently been developed; the numerical simulations reveal the bound state near the wall (Li & Ardekani 2014). The result was also consistent with the analysis of the equation of motion of squirmer borrowing the technique from dynamical systems (Ishimoto & Gaffney 2013). Even for Janus particles, it was very recent to perform numerical simulations near a wall (Uspal *et al.* 2015).

In this work, we discuss the interaction between self-propelled drops. In particular, we focus on the head-on collision between two drops. As we will discuss, the interaction has two origins: hydrodynamics and concentration overlap. The hydrodynamic interaction has been discussed in the squirmer model where only the velocity field is treated. The concentration overlap has been discussed in the field of reaction-diffusion systems where the concentration fields are analyzed without considering hydrodynamics and thus no mechanics plays a role (Ohta *et al.* 1997; Ohta 2001; Bode *et al.* 2002; Nishiura *et al.* 2003). The primary questions are which effect dominates the interaction and when crossover occurs. To answer the questions, we consider the theory for two interacting drops separated far away from each other. This is the extension of the theory for a single drop discussed in (Yabunaka *et al.* 2012; Yoshinaga 2014).

We also develop the numerical simulations of isolated as well as interacting drops. This enables us to investigate the effect of advection of the chemical component for which complete analytical argument is still missing in (Yabunaka *et al.* 2012; Yoshinaga 2014). We confirm that the convection of the chemical component does not change essential bifurcation of a single drop but suppresses the drift instability, which supports the

previous theories (Yabunaka *et al.* 2012; Yoshinaga 2014). For interacting drops, we will numerically treat dynamics of collision, which complements our theoretical calculations.

The interaction between two self-propelled particles is distinct from the conventional passive systems where particles and drops are driven by external forces (Jeffrey & Onishi 1984). The dominant hydrodynamic interaction at far field does not arise from the Stokeslet but from source doublet or stresslet depending on the $l = 1$ or $l = 2$ mode for the expansion of the slip velocity in the spherical harmonics (Lauga & Powers 2009; Pak & Lauga 2014). In addition, our system is different from the squirmer and the Janus particle; our system does not have specific polarity at the intrinsic level but spontaneously appear above the threshold of the bifurcation parameter. Consequently, the drop may change the direction of motion without rotation.

In the remaining sections, we formulate the model for chemically-driven self-propulsion using the Marangoni effect. As preparation for later arguments, in section 2, we compute the flow field and resulting velocity of the drop under given surface tension distribution. In section 3, the spontaneous motion of an isolated drop is summarized. In section 4, the hydrodynamic and concentration-mediated interactions between two drops are derived. The equations of motion for the two interacting drops are formulated in section 5. The numerical results for isolated and colliding drops are shown in section 6 and section 7, respectively. We compare the results with our theoretical analysis discussed in section 4. We conclude with section 8 by summarizing our results.

2. An isolated drop under a given concentration gradient

Before discussing the interaction between spherical drops, we first calculate the flow field around the spherical drop driven by arbitrary surface tension distribution. In the literature, the axisymmetric flow field around the drop has been studied (Young *et al.* 1959; Levan 1981; Kitahata *et al.* 2011). Here we do not assume axisymmetry of the system and the surface tension is expanded not by Legendre polynomials but by spherical harmonics as

$$\gamma(\theta, \varphi) = \sum_{l,m} \gamma_{lm} Y_l^m(\theta, \varphi). \quad (2.1)$$

The velocity fields inside and outside the drop are accordingly expanded as

$$\mathbf{v}^{(i)} = \sum_{l,m} \mathbf{v}_{lm}^{(i)} = \sum_{l,m} \left[f_{lm}^{(i)}(r) \mathbf{Y}_{lm}(\theta, \varphi) + g_{lm}^{(i)}(r) \mathbf{\Psi}_{lm}(\theta, \varphi) \right] \quad (2.2)$$

$$\mathbf{v}^{(o)} = \sum_{l,m} \mathbf{v}_{lm}^{(o)} = \sum_{l,m} \left[f_{lm}^{(o)}(r) \mathbf{Y}_{lm}(\theta, \varphi) + g_{lm}^{(o)}(r) \mathbf{\Psi}_{lm}(\theta, \varphi) \right], \quad (2.3)$$

where the vector spherical harmonics is defined using the scalar spherical harmonics $Y_l^m(\theta, \varphi)$ as

$$\mathbf{Y}_{lm} = Y_l^m \hat{\mathbf{r}} \quad (2.4)$$

$$\mathbf{\Psi}_{lm} = r \nabla Y_l^m, \quad (2.5)$$

where $\hat{\mathbf{r}}$ is a unit normal vector. Hereafter, we denote the outer and inner fields by the superscripts (o) and (i), respectively. Since the flow field is driven by a gradient of surface tension, one of the vector spherical harmonics, $\mathbf{\Phi}_{lm} = \mathbf{r} \times \nabla Y_l^m$ in the tangential direction perpendicular to $\mathbf{\Psi}_{lm}$ does not appear in this expansion. $f_{lm}(r)$ and $g_{lm}(r)$ are determined from the boundary conditions as discussed below.

We consider the spherical drop is moving with the velocity \mathbf{u} in the arbitrary direction.

The velocity is expressed at any point (θ, φ) on the drop surface as

$$\mathbf{u} = \sum_m u_m (\mathbf{Y}_{1,m}(\theta, \varphi) + \boldsymbol{\Psi}_{1,m}(\theta, \varphi)), \quad (2.6)$$

which is equivalent to

$$\mathbf{u} = \left(\sqrt{\frac{3}{4\pi}} \frac{u_{-1} - u_1}{\sqrt{2}}, i \sqrt{\frac{3}{4\pi}} \frac{-u_{-1} - u_1}{\sqrt{2}}, \sqrt{\frac{3}{4\pi}} u_0 \right) \quad (2.7)$$

in the Cartesian coordinates (see (2.11)).

We consider the velocity of the drop is slow enough to assume the zero Reynolds number and it satisfies the Stokes equation except over the surface of the drop $r = R$

$$\eta^{(i)} \nabla^2 \mathbf{v}^{(i)} - \nabla p^{(i)} = 0, \quad (2.8)$$

$$\eta^{(o)} \nabla^2 \mathbf{v}^{(o)} - \nabla p^{(o)} = 0, \quad (2.9)$$

The pressure p is determined from the incompressibility condition

$$\nabla \cdot \mathbf{v} = 0. \quad (2.10)$$

The boundary condition on $r = R$ reads

$$\mathbf{v}^{(o)} \cdot \hat{\mathbf{r}} = \mathbf{v}^{(i)} \cdot \hat{\mathbf{r}} = \mathbf{u} \cdot \hat{\mathbf{r}} \quad (2.11)$$

$$\mathbf{v}^{(o)} \cdot \hat{\mathbf{t}} = \mathbf{v}^{(i)} \cdot \hat{\mathbf{t}} \quad (2.12)$$

$$\sigma_{nt}^{(i)}(R) \hat{\mathbf{t}} = \sigma_{nt}^{(o)}(R) \hat{\mathbf{t}} + \frac{1}{R} \nabla_s \gamma \quad (2.13)$$

with the unit tangent vectors $\hat{\mathbf{t}}$. (2.11) and (2.12) are continuity of the velocity fields across the interface, and (2.13) is force balance at the interface, namely the jump of shear stress across the interface due to the force created by the inhomogeneous surface tension (Scriven 1960). The system is force-free; there is no mechanical force acting on the drop,

$$\mathbf{F} = \int dS \sigma^{(o)}(R) \cdot \mathbf{n} = 0, \quad (2.14)$$

where the integral is taken over the surface of the drop. The stress balance in the normal direction is simultaneously satisfied for the $l = 1$ mode and determines a shape of the drop for $l \geq 2$.

The solution of the Stokes equations (2.8) and (2.9) is decomposed into the two parts; one is for $l = 1$ and the other is for $l \geq 2$. For $l = 1$,

$$\mathbf{v}_{1,m}^{(i)} = u_m \left(\left[-\frac{3}{2} \left(\frac{r}{R} \right)^2 + \frac{5}{2} \right] \mathbf{Y}_{1,m} + \left[-3 \left(\frac{r}{R} \right)^2 + \frac{5}{2} \right] \boldsymbol{\Psi}_{1,m} \right) \quad (2.15)$$

$$\mathbf{v}_{1,m}^{(o)} = u_m \left[\left(\frac{R}{r} \right)^3 \mathbf{Y}_{1,m} - \frac{1}{2} \left(\frac{R}{r} \right)^3 \boldsymbol{\Psi}_{1,m} \right] \quad (2.16)$$

$$p^{(o)} = 0 \quad (2.17)$$

$$p^{(i)} = - \sum_m \frac{10\eta^{(i)}\gamma_{1,m}}{R(3\eta^{(i)} + 2\eta^{(o)})} \frac{r}{R} Y_1^m(\theta, \varphi) = - \sum_m \frac{15\eta^{(i)}u_m}{R} \frac{r}{R} Y_1^m(\theta, \varphi) \quad (2.18)$$

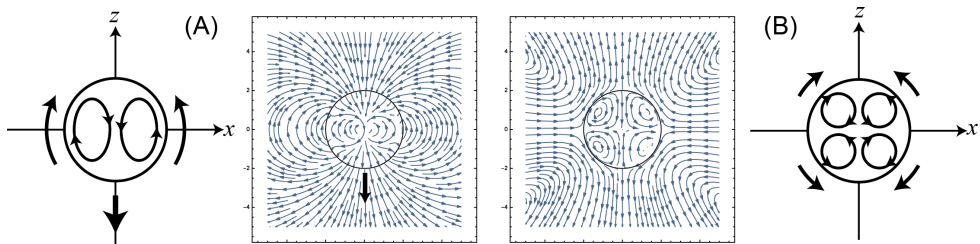


FIGURE 1. The flow field created by a isolated drop. (A) The $l = 1$ mode associated with the translational motion under $\gamma_{1,0} > 0$ given by (2.15) and (2.16). The direction of motion is shown in the thick arrow. (B) The $l = 2$ mode of the dipolar flow for $\gamma_{2,0} > 0$ given by (2.19) and (2.20). The schematic drawings of the flow fields are also shown.

and for $l \geq 2$

$$\mathbf{v}_{l,m}^{(i)} = \frac{\gamma_{lm}}{2(\eta^{(i)} + \eta^{(o)})(2l+1)} \left(l(l+1) \left[\left(\frac{r}{R} \right)^{l+1} - \left(\frac{r}{R} \right)^{l-1} \right] \mathbf{Y}_{lm} + \left[-(l+1) \left(\frac{r}{R} \right)^{l-1} + (l+3) \left(\frac{r}{R} \right)^{l+1} \right] \mathbf{\Psi}_{lm} \right) \quad (2.19)$$

$$\mathbf{v}_{l,m}^{(o)} = \frac{\gamma_{lm}}{2(\eta^{(i)} + \eta^{(o)})(2l+1)} \left(l(l+1) \left[\left(\frac{R}{r} \right)^l - \left(\frac{R}{r} \right)^{l+2} \right] \mathbf{Y}_{lm} + \left[-(l-2) \left(\frac{R}{r} \right)^l + l \left(\frac{R}{r} \right)^{l+2} \right] \mathbf{\Psi}_{lm} \right) \quad (2.20)$$

$$p^{(o)} = \sum_{l,m} \frac{\eta^{(o)} \gamma_{lm}}{R(\eta^{(i)} + \eta^{(o)})} \frac{l(2l-1)}{2l+1} \left(\frac{R}{r} \right)^{l+1} Y_l^m(\theta, \varphi) \quad (2.21)$$

$$p^{(i)} = \sum_{l,m} \frac{\eta^{(i)} \gamma_{lm}}{R(\eta^{(i)} + \eta^{(o)})} \frac{(l+1)(2l+3)}{2l+1} \left(\frac{r}{R} \right)^l Y_l^m(\theta, \varphi). \quad (2.22)$$

Because of the force-free condition, the velocity field for $l = 1$ decays as $1/r^3$ and not as $1/r$. This is the manifestation of the fact that the motion is not driven by the Stokeslet but the quadrupole (source dipole). The velocity of the drop is

$$u_m = -\frac{2\gamma_{1,m}}{3(3\eta^{(i)} + 2\eta^{(o)})}. \quad (2.23)$$

The axisymmetric case corresponds to $\gamma_{l,m} = 0$ for $m \neq 0$. The result is consistent with (Young *et al.* 1959) †. Note that the coefficient may depend on the definition of the normalization factor in the spherical harmonics.

3. Self-propelled motion of a single drop

In this section, we summarize the self-propulsive motion of an isolated drop. The details for the analysis of this model are found in (Yabunaka *et al.* 2012). We consider the dynamics of the concentration field

$$\frac{\partial c}{\partial t} + \mathbf{v} \cdot \nabla c = D\nabla^2 c - \kappa(c - c_\infty) + A\Theta(R - |\mathbf{r} - \mathbf{r}_G|). \quad (3.1)$$

† except typographical errors. See (Levan 1981; Kitahata *et al.* 2011)

The system is driven away from the equilibrium state, where the drop is stationary, by the source term described by the step function $\Theta(x)$ with the coefficient A . When $A > 0$, the drop produces chemical molecules while when $A < 0$, the drop consumes them. Note that we do not use the frame comoving with the drop. Therefore, the advection term in (3.1) describes advection only by the flow. Under the comoving frame, the term has another contribution from the fact that the drop is moving. In our model, this effect is included in the last term in (3.1).

With the spirit of the diffuse-interface model (Anderson *et al.* 1998; Hohenberg & Halperin 1977), we describe the drop as a binary mixture; $\phi = 1$ inside the drop and $\phi = -1$ outside it. The dynamics is given by Cahn-Hilliard equation with advection

$$\frac{\partial \phi}{\partial t} + \mathbf{v} \cdot \nabla \phi = \nabla \cdot L \nabla \frac{\delta F}{\delta \phi} \quad (3.2)$$

where the mobility L is assumed to be constant. The free energy is the following double-well type potential

$$F = \int_{\Omega} \left[-\frac{1}{2} \phi^2 + \frac{1}{4} \phi^4 + \frac{B(c)}{2} |\nabla \phi|^2 \right] \quad (3.3)$$

where Ω is a whole domain of the system. The interfacial energy is dependent on the concentration field $c(\mathbf{r})$. We assume the linear relation

$$B(c) = B_0 + B_1 c(\mathbf{r}) \quad (3.4)$$

characterized by two parameters B_0 and B_1 . The benefit of this approach is that we do not need to solve the Stokes equation with the moving boundary conditions. The force acting on the fluid is given by

$$\mathbf{f} = -\phi \nabla \frac{\delta F}{\delta \phi} - c \nabla \frac{\delta F}{\delta c}. \quad (3.5)$$

The force is generated by the surface tension and thus accumulated at the interface between the drop and surrounding fluid. The force is expressed in the divergence form

$$\mathbf{f} = \nabla \cdot \Pi \quad (3.6)$$

where the stress is

$$\Pi_{ij} = B(c) \nabla_i \phi \nabla_j \phi + \text{isotropic terms} . \quad (3.7)$$

The isotropic terms merely modifies the reference pressure and thus we do not discuss hereafter. (3.4) implies that the surface tension of the drop can be linearly expanded with respect to the concentration at interface when the variation of the concentration across the whole surface is small:

$$\gamma = \gamma_0 + \gamma_c c|_{\mathbf{r}=\mathbf{R}} . \quad (3.8)$$

Instead of (2.8) and (2.9), we solve the following single Stokes equation for the whole space with the force \mathbf{f} :

$$\eta \nabla^2 \mathbf{v} - \nabla p + \mathbf{f} = 0 \quad (3.9)$$

under the incompressibility condition $\nabla \cdot \mathbf{v} = 0$. We also assume $\eta^{(o)} = \eta^{(i)}$.

As discussed in (Yabunaka *et al.* 2012), the model leads to the following reduced description:

$$m \frac{d\mathbf{u}}{dt} = (-\tau_c + \tau) \mathbf{u} - g \mathbf{u} |\mathbf{u}|^2. \quad (3.10)$$

In deriving this equation, they assumed that (i) the migration of the drop due to the diffusion is much slower than that due to the flow field, (ii) the contribution due to the deformation of the drop is negligible and (iii) the convective term in (3.1) does not affect on the qualitative feature of the bifurcation. The assumption (i) can be justified when $R \gg (L\eta_0)^{1/2}$ by estimating the migration velocity due to the gradient of the concentration c as in (Yabunaka *et al.* 2012; Bhagavatula *et al.* 1997). The assumption (ii) is justified when $\gamma_c A / (\gamma\kappa) \ll 1$ as in (Yoshinaga 2014).

Here the velocity and time scales are rescaled as

$$\frac{\mathbf{u}}{D\beta} \rightarrow \mathbf{u} \quad (3.11)$$

$$\kappa t \rightarrow t. \quad (3.12)$$

The length scale is also rescaled by inverse length β defined by

$$\beta = \sqrt{\frac{\kappa}{D}}. \quad (3.13)$$

The coefficients m , τ , and g are dependent only on βR . (3.10) is characterized by the single parameter

$$\tau_c = \frac{15\eta D^2 \beta^3}{2\gamma_c A}. \quad (3.14)$$

The drop is stationary when $\tau < \tau_c$ while at $\tau = \tau_c$, the bifurcation occurs and the drop starts to move. Solving (3.10), the speed of the drop is

$$u = |\mathbf{u}| = \begin{cases} 0 & \text{for } \tau < \tau_c \\ \frac{u_0 e^{t/s_r}}{\sqrt{1 + (e^{2t/s_r} - 1) \frac{u_0^2}{u_{st}^2}}} & \text{for } \tau \geq \tau_c, \end{cases} \quad (3.15)$$

where the relaxation time s_r and the steady velocity u_{st} are

$$s_r = \frac{m}{\tau - \tau_c} \quad (3.16)$$

$$u_{st} = \sqrt{\frac{m}{g s_r}}. \quad (3.17)$$

One can see that, as the nondimensional reaction rate τ_c is getting closer to τ , the relaxation time s_r diverges.

4. Interacting Drops

When two drops or in general N drops are placed at disconnected positions, the concentration field is described by

$$\frac{\partial c}{\partial t} + \mathbf{v} \cdot \nabla c = D \nabla^2 c - \kappa(c - c_\infty) + \sum_{i=1}^N A_i \Theta(R_i - |\mathbf{r} - \mathbf{r}_{G,i}|) \quad (4.1)$$

where A_i , R_i , $\mathbf{r}_{G,i}$ and c_∞ are source strength, size, center of mass of i th drop among N drops, and the concentration at the infinitely far region. Here we consider $N = 2$ drops and we set $c_\infty = 0$. We also consider the same mean size of drops, $R_1 = R_2 = R_0$. We assume sufficiently large bare surface tension γ_0 so that the shape of the drop is always spherical. First we neglect the advection term $\mathbf{v} \cdot \nabla c$ in (4.1). The effect of advection is discussed in the last part of section 6.

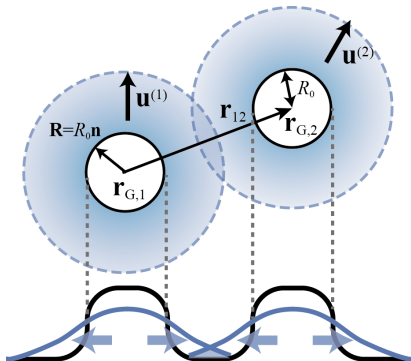


FIGURE 2. A schematic figure of interacting spherical drops. The two drops produce concentration field outside. The black line shows the drop described by the field $\phi(\mathbf{r})$. The blue (grey) lines concentration field independently created by each drop. The total concentration field $c(\mathbf{r})$ contains overlap between the two field through which the two drops interact. (bottom) the side view of the fields $\phi(\mathbf{r})$ and $c(\mathbf{r})$.

The velocity of the drop is given by (Kawasaki & Ohta 1983; Yabunaka *et al.* 2012)

$$\mathbf{u} = \frac{1}{V} \int v_n \mathbf{R} dS \quad (4.2)$$

with $V = \frac{4}{3}\pi R_0^3$. The velocity of the drop (4.2) is modified by the two effects; one is from the concentration field denoted by \mathbf{u}_c and the other is from hydrodynamic interaction \mathbf{u}_h . The velocity is then expressed as

$$\mathbf{u} = \mathbf{u}_0 + \mathbf{u}_c + \mathbf{u}_h, \quad (4.3)$$

where the first term describes the contribution of the isolated drop.

4.1. hydrodynamic interaction

First, we consider the hydrodynamic interaction. By assuming the two drops far apart from each other, we may replace the contribution of the hydrodynamic interaction \mathbf{u}_h in (4.3) by the flow field created by the second drop: Using Faxen's law (Hetsroni & Haber 1970), the hydrodynamic interaction is expressed, in terms of the flow field $\mathbf{v}^{(2)}$ generated by the second drop, as

$$\mathbf{u}_h = \mathbf{v}^{(2)} \Big|_{\mathbf{r}=\mathbf{r}_1} + \mathcal{O} \left(\nabla^2 \mathbf{v}^{(2)} \Big|_{\mathbf{r}=\mathbf{r}_1} \right). \quad (4.4)$$

The velocity is evaluated at the center of the first drop. Because of the Laplacian operating on the velocity field, the second term is negligible compared with the first term when the distance between two drops is large $r_{12} \gg R$. Close to the drift bifurcation point with its distance ϵ , the velocity of the second drop and the surface tension scale, respectively, as $u^{(2)} \sim \epsilon$ and $\gamma_{l,m} \sim \epsilon^l$. In addition, the velocity field decays with $1/r^3$ for $l = 1$ and with $1/r^2$ for $l = 2$. Therefore, it suffices to consider $l = 1$ and $l = 2$. The

flow created by the second drop is

$$\mathbf{v}_{1,m}^{(1)} \simeq u_m^{(2)} \left[\left(\frac{R_0}{r_{12}} \right)^3 \mathbf{Y}_{1,m}(\pi - \theta_{12}, \pi + \varphi_{12}) - \frac{1}{2} \left(\frac{R_0}{r_{12}} \right)^3 \mathbf{\Psi}_{1,m}(\pi - \theta_{12}, \pi + \varphi_{12}) \right] \quad (4.5)$$

$$\mathbf{v}_{2,m}^{(1)} \simeq \frac{3\gamma_{2,m}^{(2)}}{5(\eta^{(i)} + \eta^{(o)})} \left(\frac{R_0}{r_{12}} \right)^2 \mathbf{Y}_{2,m}(\pi - \theta_{12}, \pi + \varphi_{12}), \quad (4.6)$$

where θ_{12} and φ_{12} are the polar and azimuthal angles of $\mathbf{r}_2 - \mathbf{r}_1$, respectively.

4.2. concentration-mediated interaction

Next, we consider interaction between two drops by overlap of the concentration field following the approach in (Ohta *et al.* 1997; Ohta 2001) (See Figure 2). In the Fourier space, (4.1) reads

$$\frac{\partial c_{\mathbf{q}}}{\partial t} = -D(q^2 + \beta^2)c_{\mathbf{q}} + H_{\mathbf{q}}, \quad (4.7)$$

where

$$H_{\mathbf{q}} = A_1 S_q^{(1)} e^{i\mathbf{q} \cdot \mathbf{r}_{G,1}} + A_2 S_q^{(2)} e^{i\mathbf{q} \cdot \mathbf{r}_{G,2}} \quad (4.8)$$

and

$$S_q^{(1)} = S_q^{(2)} = S_q = 4\pi \frac{\sin(qR_0) - qR_0 \cos(qR_0)}{q^3} = \frac{4\pi R_0^2}{q} j_1(qR_0). \quad (4.9)$$

Here $j_n(x)$ for $n = 0, 1, 2, \dots$ are spherical Bessel functions defined in (A 2). Similar to (Yabunaka *et al.* 2012), the solution of (4.7) is expanded close to the critical point of drift bifurcation, namely for $\epsilon = u/(D\beta) \ll 1$,

$$c_{\mathbf{q}} = \frac{G_q}{D} H_{\mathbf{q}} - \frac{G_q^2}{D^2} \frac{\partial H_{\mathbf{q}}}{\partial t} + \frac{G_q^3}{D^3} \frac{\partial^2 H_{\mathbf{q}}}{\partial t^2} - \frac{G_q^4}{D^4} \frac{\partial^3 H_{\mathbf{q}}}{\partial t^3} + \dots \quad (4.10)$$

with the Green's function

$$G_q = \frac{1}{q^2 + \beta^2}. \quad (4.11)$$

After inverse Fourier transformation, the concentration c_I at the interface of a first drop is

$$c_I = c_I^{(0)}(\mathbf{r}_{G,1} + \mathbf{s}) + c_I^{(1)}(\mathbf{r}_{G,1} + \mathbf{s}) + c_I^{(2)}(\mathbf{r}_{G,1} + \mathbf{s}) + c_I^{(3)}(\mathbf{r}_{G,1} + \mathbf{s}) + \dots, \quad (4.12)$$

where

$$\begin{aligned} c_I^{(0)}(\mathbf{r}_{G,1} + \mathbf{s}) &= \frac{1}{D} \int_{\mathbf{q}} G_q \left[A_1 S_q^{(1)} e^{i\mathbf{q} \cdot \mathbf{r}_{G,1}} + A_2 S_q^{(2)} e^{i\mathbf{q} \cdot \mathbf{r}_{G,2}} \right] e^{-i\mathbf{q} \cdot (\mathbf{r}_{G,1} + \mathbf{s})} \\ &= \frac{A_1}{D} \left[Q_1^{(0)}(s) + Q_1^{\text{int}}(\theta, \varphi) \right], \end{aligned} \quad (4.13)$$

where $Q_n^{(0)}(s)$ is

$$\begin{aligned} Q_n^{(0)}(s) &= \int_{\mathbf{q}} G_q^n S_q e^{-i\mathbf{q} \cdot \mathbf{s}} \\ &= \frac{2R_0^2}{\pi} \int_0^\infty dq G_q^n q j_1(qR_0) j_0(qs). \end{aligned} \quad (4.14)$$

The contribution from interaction, $Q_n^{\text{int}}(\theta, \varphi)$ is calculated as

$$\begin{aligned} Q_n^{\text{int}}(\mathbf{s}) &= \frac{A_2}{A_1} \int_{\mathbf{q}} G_q S_q e^{-i\mathbf{q} \cdot (\mathbf{s} + \mathbf{r}_{G,1} - \mathbf{r}_{G,2})} \\ &= \frac{2R_0^2 A_2}{\pi A_1} \int_0^\infty dq G_q^n q j_0(q|\mathbf{s} + \mathbf{r}_{G,1} - \mathbf{r}_{G,2}|) j_1(qR_0), \end{aligned} \quad (4.15)$$

Using the addition theorem of Spherical Bessel Function (Watson 1922), we have

$$j_0(q|\mathbf{s} + \mathbf{r}_{G,1} - \mathbf{r}_{G,2}|) = \sum_{l=0}^{\infty} (2l+1) j_l(qs) j_l(qr_{12}) P_l(\cos \phi_{s12}), \quad (4.16)$$

where $r_{12} = |\mathbf{r}_{G,2} - \mathbf{r}_{G,1}|$ and ϕ_{s12} is the angle between \mathbf{s} and $\mathbf{r}_{12} = \mathbf{r}_{G,2} - \mathbf{r}_{G,1}$. The Legendre polynomial is also decomposed as (Arfken *et al.* 1968)

$$P_l(\cos \phi_{s12}) = \frac{4\pi}{2l+1} \sum_{m=-l}^l Y_l^m(\theta, \varphi) Y_l^{m*}(\theta_{12}, \varphi_{12}). \quad (4.17)$$

Then (4.15) becomes

$$Q_n^{\text{int}}(\mathbf{s}) = \frac{8R_0^2 A_2}{A_1} \sum_{l=0}^{\infty} \sum_{m=-l}^l \int_0^\infty dq G_q^n q j_1(qR_0) j_l(qs) j_l(qr_{12}) Y_l^m(\theta, \varphi) Y_l^{m*}(\theta_{12}, \varphi_{12}). \quad (4.18)$$

The next order in expansion of the concentration field is

$$\begin{aligned} c_I^{(1)}(\mathbf{r}_G + \mathbf{s}) &= -\frac{A_1}{D^2} \int_{\mathbf{q}} G_q^2 \left[(i\mathbf{q} \cdot \mathbf{u}^{(1)}) S_q^{(1)} e^{i\mathbf{q} \cdot \mathbf{r}_{G,1}} + \frac{A_2}{A_1} (i\mathbf{q} \cdot \mathbf{u}^{(2)}) S_q^{(2)} e^{i\mathbf{q} \cdot \mathbf{r}_{G,2}} \right] e^{-i\mathbf{q} \cdot (\mathbf{r}_G + \mathbf{s})} \\ &= u_i^{(1)} \frac{A_1}{D^2} \left[n_i^{(0)} \frac{\partial Q_2^{(0)}}{\partial s} \right] + u_i^{(2)} \frac{A_2}{D^2} \frac{\partial}{\partial s_i} Q_2^{\text{int}} \end{aligned} \quad (4.19)$$

where the first term is the same as the velocity without the second drop.

The velocity is expressed by the sum of the velocity originated from normal and tangential forces in (3.9) on the surface of the drop. Each force is the sum of the isolated drop and the contribution from the interaction,

$$\mathbf{u}_0 + \mathbf{u}_c = \mathbf{u}_1 + \mathbf{u}_2 \quad (4.20)$$

where \mathbf{u}_1 and \mathbf{u}_2 are contribution from the normal and tangential forces, respectively. Each velocity is decomposed as

$$\mathbf{u}_1 = \mathbf{u}_1^{(0)} + \mathbf{u}_1^{\text{int}} \quad (4.21)$$

$$\mathbf{u}_2 = \mathbf{u}_2^{(0)} + \mathbf{u}_2^{\text{int}} \quad (4.22)$$

At each order in the expansion of (4.12), the Stokes equation (3.9) is solved using tensor

$$\mathbf{T}_{ij} = \frac{1}{8\pi\eta} \left[\frac{1}{r} \delta_{ij} + \frac{x_i x_j}{r^3} \right] \quad (4.23)$$

and the interaction is expanded accordingly as $\mathbf{u}_1^{\text{int}} = \mathbf{u}_1^{\text{int},0} + \mathbf{u}_1^{\text{int},1} + \mathbf{u}_1^{\text{int},2} + \dots$ with respect to the magnitude of the velocity of the second drop. The lowest-order contribution

from the interaction between spherical drops to the velocity is

$$\begin{aligned} u_{i,1}^{\text{int},0} &= \frac{\gamma_c R_0}{\Omega} \int da \int da' n_i(a) \mathbb{T}_{jk}(a, a') n_j(a) n_k(a') \left(-\frac{2}{R_0} \right) c_I^{(0)}(a') \\ &= -\frac{64\gamma_c R_0^2 A_2 a_{1,0}^{(1)}}{15\eta D} \int_0^\infty dq q G_q j_1(qR_0) j_1(qr_{12}) j_1(qR_0) N_i(\theta_{12}, \varphi_{12}) \end{aligned} \quad (4.24)$$

where $a_{1,0}^{(1)} = 3/(4\pi)$ and

$$N(\theta_{12}, \varphi_{12}) = \hat{\mathbf{r}}_{12} = \frac{\mathbf{r}_{12}}{|\mathbf{r}_{12}|} = \frac{\mathbf{r}_{2,G} - \mathbf{r}_{1,G}}{|\mathbf{r}_{2,G} - \mathbf{r}_{1,G}|} \quad (4.25)$$

is the normal vector pointing the second drop from the first drop. The velocity from tangential force is

$$\begin{aligned} u_{i,2}^{\text{int},0} &= \frac{\gamma_c R_0}{\Omega} \int da \int da' n_i(a) \mathbb{T}_{jk}(a, a') n_j(a) [\delta_{kl} - n_k(a') n_l(a')] \nabla_l c_I^{(0)} \\ &= \frac{\gamma_c R_0^2}{5\Omega\eta} \int da' [\delta_{ij} - n_i(a') n_j(a')] \nabla_j c_I^{(0)}(a'). \end{aligned} \quad (4.26)$$

The first contribution that comes from $Q_1^{(0)}(s)$ in Eq. (4.13) vanishes since $(\delta_{ij} - n_i(a') n_j(a')) n_j = 0$, and the second contributions comes from $Q_1^{\text{int}}(\theta, \varphi)$ in Eq. (4.13) is given by

$$u_{i,2}^{\text{int},0} = \frac{8\gamma_c R_0^3 A_2 a_{0,1}^{(1)}}{5\eta D} \int_0^\infty dq q G_q j_1(qR_0) j_1(qr_{12}) j_1(qR_0) N_i(\theta_{12}, \varphi_{12}) \quad (4.27)$$

where $a_{0,1}^{(1)} = (2/R_0) a_{1,0}^{(1)}$. Combining (4.24) and (4.27), we obtain

$$\begin{aligned} \mathbf{u}^{\text{int}} &= -\nabla_{r_1} U_0(r_{12}) \\ &= -\frac{\gamma_c A_2}{\eta D \beta^2} k_1(\beta r_{12}) g_0(\beta R_0) \frac{\mathbf{r}_2 - \mathbf{r}_1}{|\mathbf{r}_2 - \mathbf{r}_1|} \end{aligned} \quad (4.28)$$

where $k_1(x)$ is the modified spherical Bessel function defined as $k_1 = -\frac{d}{dx} \frac{\exp(-x)}{x}$ and we may express the *potential* as

$$U_0(r_{12}) = \frac{16a_{1,0}^{(1)} \gamma_c R_0^2 A_2}{15\eta D} \int_0^\infty dq G_q j_1(qR_0) j_0(qr_{12}) j_1(qR_0). \quad (4.29)$$

Here we have used (A 4). Using (A 5) and (A 7), we obtain

$$U_0(r_{12}) = \frac{\gamma_c A_2}{\eta D \beta^3} g_0(\hat{R}_0) k_0(\beta r_{12}) \quad (4.30)$$

with $\hat{R}_0 = \beta R_0$ and

$$g_0(\hat{R}_0) = -\frac{2a_{1,0}^{(1)} \pi}{15\hat{R}_0^2} \left[-2 \left(\hat{R}_0^2 + 2 \right) \cosh(2\hat{R}_0) + 5\hat{R}_0 \sinh(2\hat{R}_0) + 4 \right]. \quad (4.31)$$

The plot of g_0 is shown in Figure 3. From (3.14), the activity of the first drop is controlled by $\gamma_c A_1$. In order to exhibit the instability for an isolated drop, the activity $\gamma_c A_1$ must be positive. Under the condition, the inequality $g_0(\hat{R}_0) \geq 0$ implies that the *potential* is repulsive when $A_1 A_2 > 0$ and attractive when $A_1 A_2 < 0$.

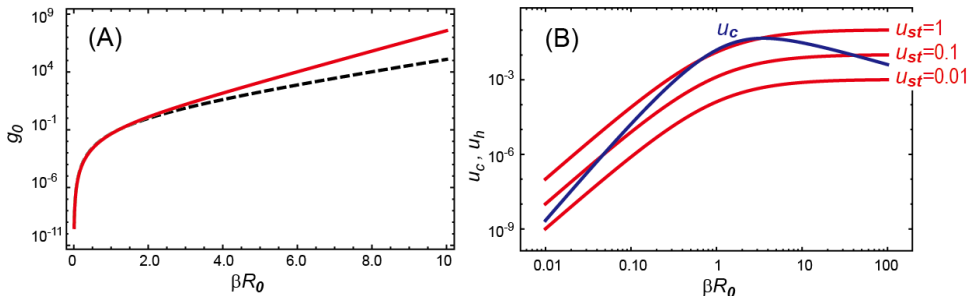


FIGURE 3. (A) The normalized concentration-mediated interaction as a function of the normalized size of the drop, βR_0 . The plot is on a semi logarithmic scale. The solid (red) line shows $g_0(\beta R_0)$ in (4.28) and the dashed (black) line corresponds to the result under the far-field approximation. (B) The log-log plot of the typical hydrodynamic u_h and concentration-mediated u_c interactions for different normalized size βR_0 of the drops. The interactions are evaluated at the characteristic length scale $r_{12} = 2R_0 + \beta^{-1}$. For the hydrodynamic interaction, the steady velocity is decreased from the top to bottom lines.

4.3. Far-Field Approximation

When the distance between two drops is significantly larger than the size of the drop, that is $r_{12} \gg R_0$

$$|\mathbf{s} - \mathbf{r}_{12}| = r_{12} \left[1 + \frac{s^2}{r_{12}^2} - \frac{2\mathbf{s} \cdot \mathbf{r}_{12}}{r_{12}^2} \right]^{1/2} \simeq r_{12} \left[1 - \frac{\mathbf{s} \cdot \mathbf{r}_{12}}{r_{12}^2} + \left(\frac{s^2}{2r_{12}^2} - \frac{(\mathbf{s} \cdot \mathbf{r}_{12})^2}{2r_{12}^4} \right) + \dots \right]. \quad (4.32)$$

Then instead of using (4.16), we may expand as

$$j_0(q|\mathbf{s} - \mathbf{r}_{12}|) \simeq j_0(qr_{12}) - qr_{12}j_0'(qr_{12}) \frac{\mathbf{s} \cdot \mathbf{r}_{12}}{r_{12}^2} + \frac{qr_{12}}{2} \left[j_0''(qr_{12}) \frac{s^2}{r_{12}^2} + (-j_0'(qr_{12}) + qr_{12}j_0''(qr_{12})) \frac{(\mathbf{s} \cdot \mathbf{r}_{12})^2}{r_{12}^4} \right] + \dots \quad (4.33)$$

With this expansion, we will use (4.15) instead of (4.18). From the zeroth-order expansion of the concentration field, the velocity of the drop due to normal force becomes

$$u_{i,1}^{\text{int},0} = -\frac{16R_0^3\gamma_c A_2}{15\pi\Omega\eta D} \int da' n_i^{(0)}(a') \int dq G_q q j_0(q|\mathbf{R}(a') - \mathbf{r}_{12}|) j_1(qR_0). \quad (4.34)$$

For the spherical drop, $\mathbf{R}(a') = R_0\mathbf{n}(a')$, and therefore, the even number of \mathbf{s} in (4.33) does not contribute the integral. The isotropic term in (4.33) does not make a contribution for $c_i^{(0)}$. At the lowest order, the velocity becomes

$$u_{i,1}^{\text{int},0} \simeq -\frac{16R_0^2\gamma_c A_2}{15\pi\eta D} N_i(\theta_{12}, \varphi_{12}) \int dq G_q q^2 R_0 j_1(qr_{12}) j_1(qR_0). \quad (4.35)$$

The contribution from the tangential force is

$$\begin{aligned} u_{i,2}^{\text{int},0} &= \frac{\gamma_c R_0^2 A_1}{5\Omega\eta D} \int da' \left[\delta_{ij} - n_i^{(0)}(a') n_j^{(0)}(a') \right] \nabla_j Q_1^{\text{int}} \\ &= \frac{4\gamma_c R_0^3 A_2}{5\pi\eta D} N_j(\theta_{12}, \varphi_{12}) \int dq G_q q^2 j_1(qR_0) j_1(qr_{12}). \end{aligned} \quad (4.36)$$

We obtain the similar interaction $\mathbf{u}^{\text{int},0} \sim k_1(\beta r_{12})\mathbf{N}$ as (4.28) with different functional form of $g_0(\beta R_0)$ even under the far-field approximation. Figure 3 shows $g_0(\beta R_0)$ in (4.28)

and under the far-field approximation. For $\beta R_0 \ll 1$, the two results agree while there is deviation for $\beta R_0 \gg 1$. We are also analytically able to confirm that the (4.28) approaches the above expression of $u_i^{\text{int},0}$ in the far field limit $r_{12} \gg R_0$ using the following relation that holds in the far field limit:

$$3 \int dq q G_q (j_1(qR_0))^2 j_1(qr_{12}) \simeq R_0 \int dq q^2 G_q j_1(qR_0) j_1(qr_{12}). \quad (4.37)$$

The higher orders term with respect to the magnitude of the velocity of the second drop are systematically computed; for the first order in expansion, the velocity is expressed as

$$u_{i,1}^{\text{int},1} = -\frac{8R_0\gamma_c A_2}{15\Omega\eta D^2} u_j^{(2)} \int da' n_i^{(0)}(a') \frac{\partial}{\partial s_j} Q_2^{\text{int}}. \quad (4.38)$$

Similarly, the other higher order terms in expansion contain the larger number of derivative with respect to s_i . At the far-field limit, the first term in (4.33) does not depend on s_i and therefore the gradient with respect to s_i vanish for higher order terms. At the next order, Q_n^{int} is linear in \mathbf{s} and therefore the higher order terms do not contribute to the velocity. The higher-order terms start to appear from the third term in (4.33). The same argument is also applied to the tangential force. It is also the case, from the symmetry, that this term should vanish for the second term in (4.33). Indeed, the integral has the odd number of normal vector and thus vanishes. We note that the shape of the first drop may also affect on the velocity of the first drop through the interaction in general cases, although we have considered only a spherical drop.

5. collision of two particles

In the previous sections, we have discussed two-body interaction. The results give kinetic rules for position ($\mathbf{x}^{(\alpha)}$) and velocity ($\mathbf{u}^{(\alpha)}$) of the α th drop ($\alpha = 1, 2$). We assume there is no viscosity contrast, that is, $\eta^{(o)} = \eta^{(i)}$. The kinetic equations are

$$\frac{d\mathbf{x}^{(1)}}{dt} = \mathbf{u}^{(1)} \quad (5.1)$$

$$m \frac{d\mathbf{u}^{(1)}}{dt} = (\tau - \tau_c) \mathbf{u}^{(1)} - g |\mathbf{u}^{(1)}|^2 \mathbf{u}^{(1)} + \mathbf{u}_c + \mathbf{u}_h, \quad (5.2)$$

where the interactions due to concentration overlap and hydrodynamics are, respectively,

$$\mathbf{u}_c = -\nabla_{\mathbf{r}_1} U_0(r_{12}) = -\frac{\gamma_c A_2}{\eta D \beta^2} g_0(\beta R_0) k_1(\beta r_{12}) N_i \quad (5.3)$$

$$\mathbf{u}_h = \left(\frac{R}{r_{12}}\right)^3 \left[-\frac{1}{2} \delta_{ij} + \frac{3}{2} \mathbf{N}\mathbf{N} \right] \cdot \mathbf{u}^{(2)} + \mathcal{O}\left(\left(\frac{R}{r_{12}}\right)^2 \mathbf{S}^{(2)} \cdot \mathbf{N}\right) \quad (5.4)$$

with the normal directional vector from the second drop to the first drop (4.25). The coefficients m , τ , and g are found in (Yabunaka *et al.* 2012). (5.2) is an equation for velocity since *effective mass* m has a dimension of time. The equation of motion for the second drop is obtained by interchanging the indices $1 \leftrightarrow 2$. S_{ij} is *dipolar* concentration distribution created around the drop, $S_{ij} = (R_0/\Omega) \int [n_i(a)n_j(a) - (1/3)\delta_{ij}] c(a) da$. This second moment of the concentration field arises both from ellipsoidal deformation and self-propulsion (Yoshinaga 2014). Since we consider a spherical drop and close to the drift bifurcation point, $S_{ij} \sim \epsilon^2$, the contribution of the second term in (5.4) is negligible. The sign of the coefficients is $-(\gamma_c A_2)/(\eta D \beta^2) g_0(\beta R_0) k_1(\beta r_{12}) < 0$ so that two drops are repelling each other.

For head-on collision, the hydrodynamic interaction is repulsive while when two drops move away from each other, the interaction becomes attractive. This is in contrast with isotropic concentration-mediated interaction. Since the steady velocity of the drop is small close to the critical point, the interaction created by the concentration field is stronger than that by the hydrodynamics. This is shown in Figure 3. Although the theoretical assumptions that we have made to calculate the interactions are not completely justified especially during collision, we will show in the following sections semi-quantitative agreement with our numerical results.

6. Numerical simulations: single drop

We numerically solve the dynamics of drop in (3.2) and the flow field in (3.9). For the convenience in numerics, we use the following equation for the dynamics of the concentration field yields similar to (4.1)

$$\frac{\partial c}{\partial t} + \mathbf{v} \cdot \nabla c = D\nabla^2 c - \kappa c + \frac{1}{2}A(\phi(\mathbf{r}) + 1). \quad (6.1)$$

We assume axisymmetric system where the motion of the drop is confined along the z -axis. The whole space is discretized in the cylindrical coordinates with $N_z = 96$ and $N_r = 48$ mesh points in z - and radial (r -) directions. The mesh size is chosen as $\Delta z = \Delta r = 1$ and the time step is $\Delta t = 0.002$. The equations (6.1) and (3.2) are discretized using the forward Euler method. We imposed the periodic boundary condition in z -direction and, at $r = N_r$, the slip boundary condition $\partial_r v_z = 0$ and $v_r = 0$, the non-wetting boundary condition $\partial_r \phi = 0$ the no-flux boundary condition $\partial_r \frac{\delta f}{\delta \phi} = 0$ and $\partial_r c = 0$. The Stokes equation is solved with the relaxation method; at given force $\mathbf{f}(\mathbf{r})$, (3.9) is solved by introducing the virtual time derivative dv/dt in the equation and relaxing until steady states. At each step in the virtual time domain, the pressure is also relaxed to the steady value so that the incompressibility condition is satisfied. (i) As a way of discretization, we employed the staggered lattice method where the r and z component of a flux are defined at the lattice point $((i + 1/2)\Delta r, j\Delta z)$ and $(i\Delta r, (j + 1/2)\Delta z)$, respectively, for $i = 0, \dots, N_r - 1$ and $j = 0, \dots, N_z - 1$. (ii) In order to quickly prepare initial conditions that are stationary under Eq. (6.1) and Eq. (3.2) with $\mathbf{v} = \mathbf{0}$, we solved the following equations

$$\frac{\partial c}{\partial t'} = \alpha \left[D\nabla^2 c - \kappa c + \frac{1}{2}A(\phi(\mathbf{r}) + 1) \right], \quad (6.2)$$

$$\frac{\partial \phi}{\partial t'} = -\frac{\delta F}{\delta \phi} + \left\langle \frac{\delta F}{\delta \phi} \right\rangle, \quad (6.3)$$

with $\alpha = 20$ and $\Delta t' = 0.01$ until $t' = 160$, starting from $c = 0$ and $\phi = -\tanh(R - |\mathbf{r} - \mathbf{r}_{G,1}|) + 0.05$ at $t' = 0$. We add a noise with small amplitude to this initial condition to investigate self-propelled motion of a drop with spontaneous symmetry breaking.

First we drop the advection term in (6.1) to compare numerical results with the theoretical prediction (Yabunaka *et al.* 2012) directly. We vary the viscosity η to realize self-propulsive motion under fixed $R = 16$, $B_0 = 0.2$, $B_1 = 0.5$, $D = 0.5$, $A = 0.08$, $\kappa = 0.005$, and $L = 1$. Here $\beta = \sqrt{\frac{\kappa}{D}} = 0.1$. We confirmed that this choice of the parameters satisfies the assumptions below Eq. (3.10). With these parameters, the critical value of the viscosity is $\eta_c \simeq 1.742$ using (3.14). In order to estimate the critical value, we need to evaluate the surface tension and γ_c . When the interface is sharp and the value

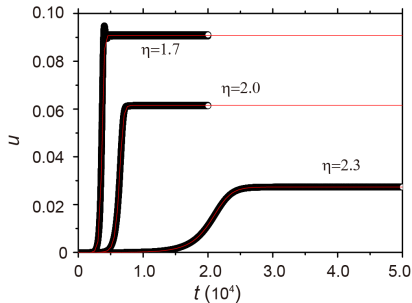


FIGURE 4. Self-propulsive velocity of a single drop. The velocity of the drop as a function of time is shown by the circles (numerical simulation) and the line (theory in (3.15)).

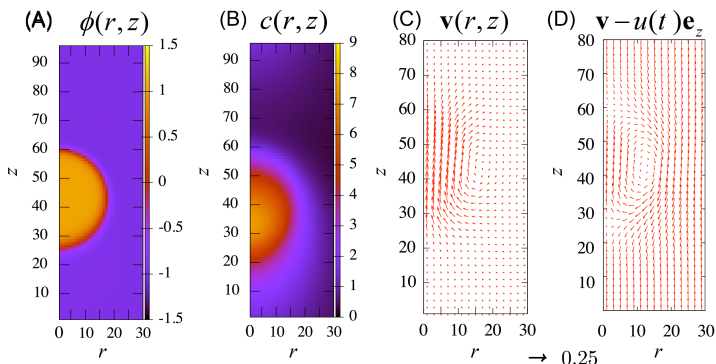


FIGURE 5. The drop $\phi(\mathbf{r})$ (A), the concentration field $c(\mathbf{r})$ (B), and the velocity field $\mathbf{v}(\mathbf{r})$ in the laboratory frame (C) and in the drop frame (D) for $\eta = 1.5$ and $t = 3168$ during the steady state. The self-propulsive velocity is $u = 0.109$.

of $c(\mathbf{r})$ at the interface is unique, then $\gamma = \frac{2\sqrt{2B(c)}}{3}$ and $\gamma_c = \frac{\sqrt{2B_1}}{3\sqrt{B(c)}}$. However, since we use a diffuse interface model, the concentration at the interface *region* varies in space. The surface tension is

$$\gamma = \int B(c) \left(\frac{\partial \phi}{\partial n} \right)^2 dn \quad (6.4)$$

where $\partial/\partial n$ is the spatial derivative along the normal direction to the interface. We numerically estimate (6.4) and compare with (3.8) to obtain $\gamma_c \sim 0.510$.

When $\eta < \eta_c$, the stationary state becomes unstable and the drop starts to move. The velocity of the drop gradually increases and reaches to its steady value as in Figure 4. During the self-propulsive motion, the concentration field is distorted around the drop shown in Figure 5. Clearly, the two centers of mass, for the drop and for the concentration, are shifted and thus the symmetry of the $\pm z$ directions is broken. The velocity field during the motion is shown in Figure 5. The velocity field in the drop frame shows circular flow corresponding to the $l = 1$ mode in Figure 1. The velocity field decays faster than $1/r$ around the drop suggesting that the motion is generated by the source dipole and not by Stokeslet.

The relaxation of the velocity is monotonic and well fitted with Eq. (3.17) when the viscosity η is close to the critical value. This is consistent with the theoretical result of (3.15). In the case of η much lower than the critical value, however, the relaxation of the velocity is not monotonic but with a small oscillation for $\eta = 1.7$ in Figure 4.

This may arise from an additional time scale involved and truncation in the expansion of (4.10) is not completely satisfied. The steady velocity and the relaxation time are plotted in Figures 6 and 7, respectively. As the viscosity η decreases, that is τ_c decreases, the self-propulsive speed increases. Close to the critical point, the speed increases as $u \sim |\eta_c - \eta|^{1/2}$ as predicted by the theory in (3.15). As the viscosity approaches the critical value from below, the relaxation time diverges. Figure 7 shows the relaxation time in numerical simulations.

We evaluate the scaled coefficients m, τ, g ($\hat{m}, \hat{\tau}, \hat{g}$ in (Yabunaka *et al.* 2012)) from the numerical results as follows: In terms of the non-scaled coefficients M, T, G (m, τ, g in (Yabunaka *et al.* 2012)), the relaxation time and the steady velocity are expressed, respectively, as

$$s_r = \frac{M}{T-1} \quad (6.5)$$

$$u_{st} = \sqrt{\frac{T-1}{G}}. \quad (6.6)$$

Since $T \sim \eta^{-1}$, the above expression of s_r predicts the divergence of the relaxation time near the threshold, which accords with the numerical results. Using $\eta_c = 2.395$, we can estimate $T-1 \sim 0.19$ for $\eta = 2.0$. From the above equations, we can estimate $G \sim 49.4$ and $M \sim 96.9$. Then after rescaling the parameters in (Yabunaka *et al.* 2012), we obtain

$$g = \tau_c (D\beta)^2 G = 0.0112, \quad (6.7)$$

$$m = MD\beta^2\tau_c = 0.044. \quad (6.8)$$

These values of m and g agree with theoretical predictions in (Yabunaka *et al.* 2012) with $\beta R = 1.6$. In the same way, we evaluated g and m for other values of η near η_c and found that they are almost constant, which is consistent with theoretical predictions as shown in Figure 8.

The advection term in (6.1) does not modify the qualitative feature of the transition; we found that, when $\eta < \eta_c = 0.2833$, the stationary state becomes unstable and the drop starts to move. In addition, Figures 6 and 7 show the advection does not modify the scaling behavior of the steady velocity near the critical point. Both with and without the advection term, the steady velocity grows as $|\eta - \eta_c|^{1/2}$. The relaxation time is also diverging near the bifurcation point. We note that the critical point $\eta_c = 0.2833$ is much smaller than $\eta_c = 2.835$ for the absence of the advection. In (Yabunaka *et al.* 2012), the effect of the advection is only treated in the limit $\beta R \rightarrow 0$ and it is predicted that, in presence of the advection, the drift instability is suppressed but the bifurcation behavior is not changed essentially. Thus our numerical results with $\beta R = 1.6$ agree with the theoretical prediction in $\beta R \rightarrow 0$ qualitatively, although the theory does directly not apply to our case.

7. Numerical simulations: interaction

With the same numerical method as in the previous section for an isolated drop, we carried out the numerical simulations of two drops. The whole space is discretized in the cylindrical coordinates with $N_z = 200$ and $N_r = 48$ mesh points in z - and radial (r -) directions. The mesh size is chosen as $\Delta z = \Delta r = 1$ and the time step is $\Delta t = 0.002$ for $\eta > 1.9$ and $\Delta t = 0.001$ for $\eta < 1.9$. We apply the same way to prepare the initial condition but with $\phi = \tanh(R - |\mathbf{r} - \mathbf{r}_{G,1}|) + \tanh(R - |\mathbf{r} - \mathbf{r}_{G,2}|) - 2 + 0.05$ with $\mathbf{r}_{G,1} = 29$ and $\mathbf{r}_{G,2} = 171$.

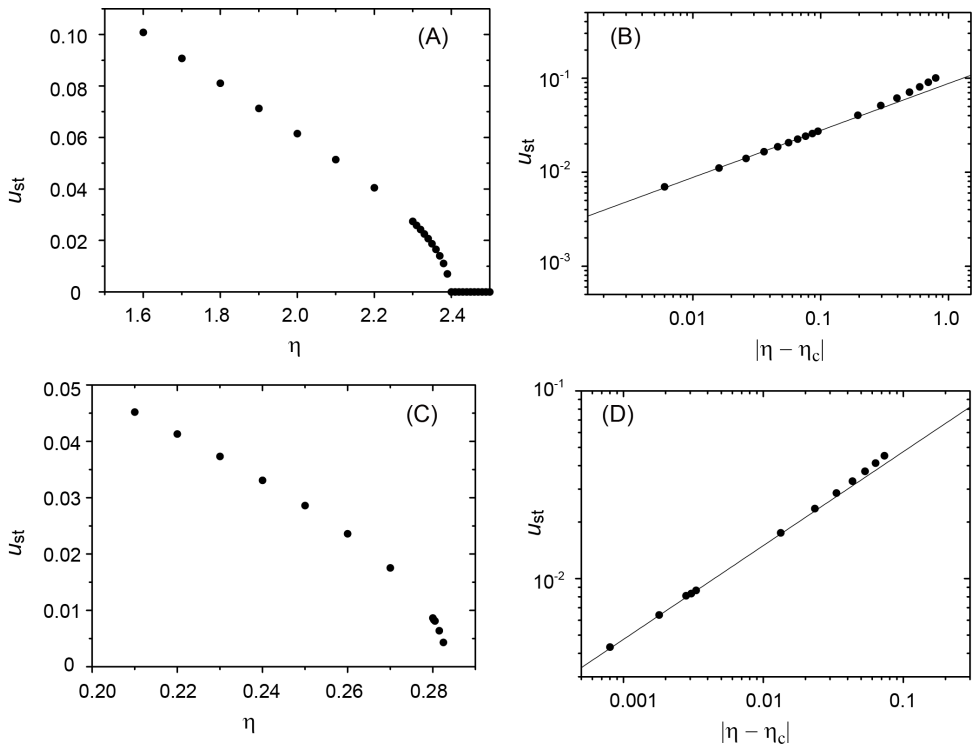


FIGURE 6. The steady velocity u_{st} with varying viscosity η (τ_c). (A,B) without advection and (C,D) with advection of the third dilute component. The log-log plots of the steady velocity and the distance from the critical points are shown in (B) and (D). The solid lines show the exponent $u_{st} \sim |\eta - \eta_c|^{1/2}$.

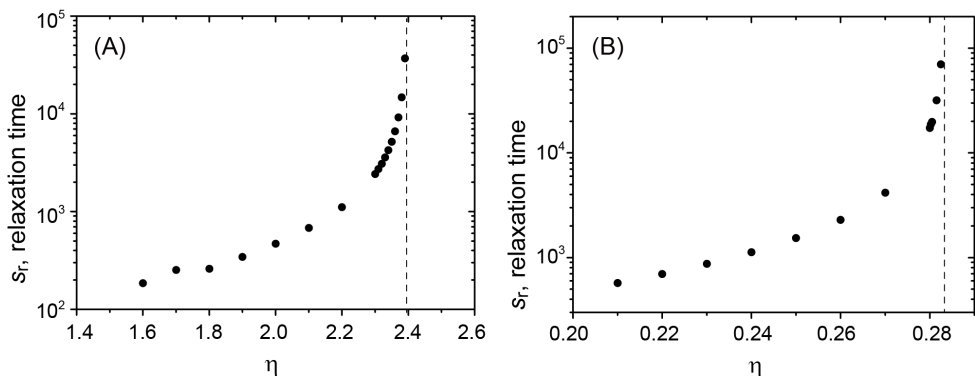


FIGURE 7. The relaxation time to reach the steady velocity. (A) without advection and (B) with advection of the third dilute component. The vertical dashed lines correspond to the critical viscosity.

Figure 9 shows the trajectory of the two centers of mass of the interacting particles. There are two distinct dynamics for collision: fusion and reflection. When the viscosity η is far below the critical point, the two drops approach and eventually they merge. On the other hand, when η is close to the critical point, the two drops do not merge even when they are approaching, but they reflect and move toward opposite directions. Surprisingly, the latter collision is elastic despite the fact that the system is dissipative. The drops are

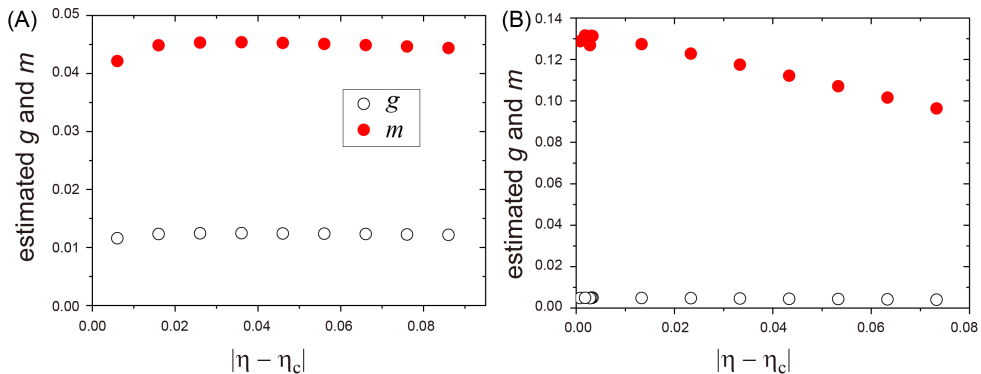


FIGURE 8. Numerically estimated coefficients g and m . (A) without advection and (B) with advection of the third dilute component.

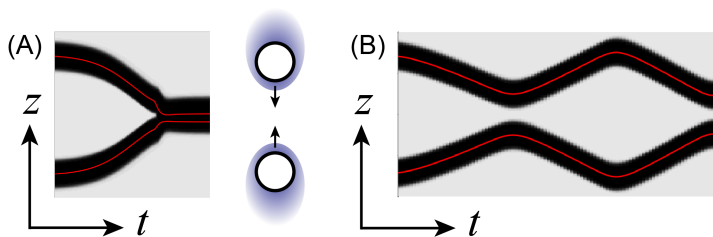


FIGURE 9. The trajectories of two colliding drops for (A) $\eta = 1.5$ and (B) $\eta = 2.3$. The slices of the field ϕ at $t = 0$ are superposed for the direction of time. The darker (brighter) region corresponds to $\phi = 1$ ($\phi = -1$). The solid lines show the trajectories of the centers of the drops. Because of the periodic boundary condition, the drops reaching the top or bottom boundaries are reflected by the interactions with image drops outside the simulation box.

moving with the same speed after collision as before collision. This could be understood from our reduced description (3.10) where *friction* vanishes as τ_c (that is proportional to η as shown in (3.14)) approaches to τ . Thus, the drop behaves as if it were in a conserved system because of the balance between dissipation and energy injection creating chemical production. This is in contrast with the squirmer model and Janus particle model where there is no *inertia* time in the equation of motion. We note that similar elastic behavior is also reported for pulse collision in reaction diffusion systems (Ohta *et al.* 1997).

In order to clarify the origin of the interaction, we solve the reduced equation for the relative position $\xi = z^{(1)} - z^{(2)}$ between the two drops obtained from (5.1) and (5.2)

$$m \frac{\partial^2 \xi}{\partial t^2} = \frac{\partial \xi}{\partial t} \left(\tau - \tau_c - \frac{g}{4} \left| \frac{\partial \xi}{\partial t} \right|^2 \right) - 2U'_0(\xi) - \left(\frac{R}{\xi} \right)^3 \frac{\partial \xi}{\partial t} \quad (7.1)$$

with the initial conditions same as the full numerical simulations. The parameters in (7.1) are obtained from the result of a single drop, and thus there is no fitting parameter in the equation. The result for $\eta = 2.3$ (Figure 9(B)) is shown in Figures 10 (A) and (B). We obtain a quite good agreement between the results of the reduced equation and the original model. It is also found that the overall feature of the evolution of \mathbf{u} is dominated by the concentration-mediated interaction although the hydrodynamic interaction gives some correction on it. We plot the contribution from the hydrodynamic ($\sim \xi^{-3}$) and concentration-mediated interactions ($\sim U'_0(\xi)$) in Figure 10. In fact, for the most of the region, u_c dominates u_h . However, the hydrodynamic interaction dominates for $\xi \gg$

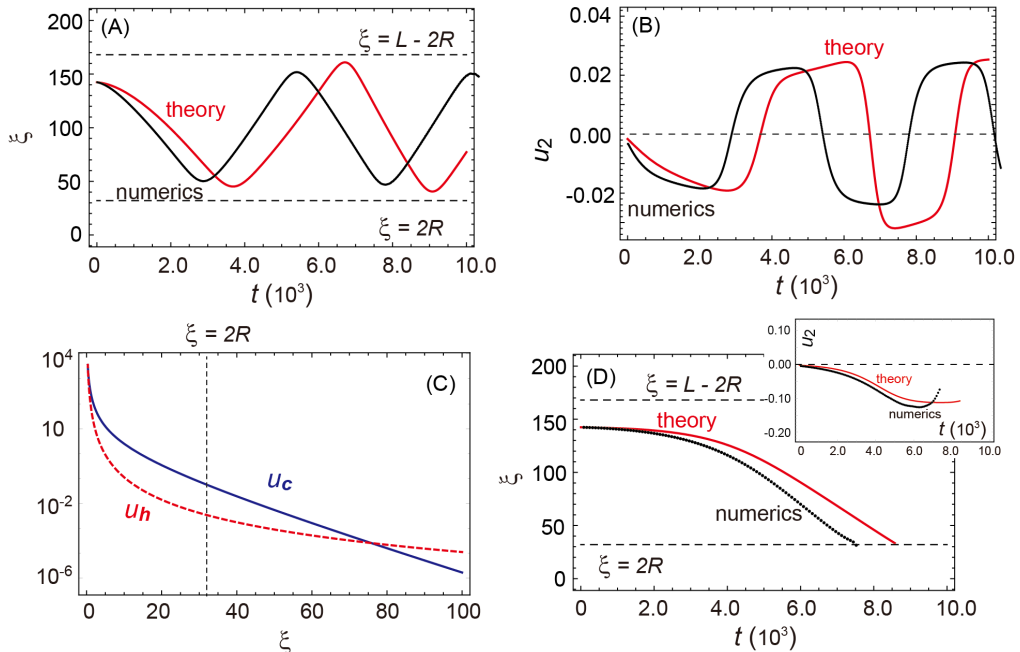


FIGURE 10. Comparison between reduced equations ((5.2) and (7.1)), and the full model for $\eta = 2.3$ (A-C) and $\eta = 1.5$ (D). (A) The distance $\xi = |z^{(1)} - z^{(2)}|$ between two drops as a function of time, (B) velocity of the second drop, and (C) the dependence of separation distance on the hydrodynamic u_h and concentration-mediated u_c interactions. u_h is estimated from the steady velocity u_{st} . (D) The distance between two drops for $\eta = 1.5$ and (inset) velocity of the second drop.

80, since the hydrodynamic (concentration-mediated) interaction decays algebraically (exponentially). For $\eta = 1.5$ (Figure 9(A)), we also solved (7.1) as shown in Figure 10(D) and found that ξ becomes less than $2R$, which suggests fusion of the drops and agrees with the results of numerical simulation of the original model.

This result is consistent with the following rough estimate of the relative magnitudes of these two interactions: The magnitude of the hydrodynamic interaction is estimated as

$$|\mathbf{u}_h| = \left(\frac{R}{\xi}\right)^3 u_j^{(2)} \sim u_{st} \left(\frac{R}{\xi}\right)^3, \quad (7.2)$$

where the typical steady state self-propelling velocity is given by $u_{st} \sim 0.02$. The magnitude of the concentration-mediated interaction is

$$|\mathbf{u}_c| \sim \frac{15D\beta}{2\tau_c} g_0(\hat{R}_0) k_1(\beta\xi), \quad (7.3)$$

where $g_0(\hat{R}_0 = 1.6) \sim 0.39$. If we set $\xi = 2R$, $k_1(\beta\xi) \sim 0.0167$, then $\mathbf{u}_c \sim 0.213$ and $\mathbf{u}_h \sim 0.0025$. This also confirms that the magnitude of the concentration-overlap-mediated interaction is larger than that of the hydrodynamic interaction.

8. Summary

We have developed the theory of collision between two self-propelled drops driven by chemical reactions. Close to the bifurcation point between stationary and self-propelled

states, the collision is elastic while away from the point, fusion occurs. The interactions originate from hydrodynamics and overlap of the concentration field. The both interactions are repulsive during head-on collision if the chemical reactions of the two drops have same sign in terms of production or consumption. We found that the concentration-mediated interaction dominates the collision dynamics. Our analytical calculation is confirmed semi-quantitatively by the numerical results.

We stress inertia-like and nonlinear terms naturally appear in the reduced description (3.10). These effects are confirmed by the numerical results where the self-propulsion indeed occurs with the divergence of relaxation time. The steady velocity obtained from the distance from the critical point also fits with our theory. During the collision of two drops, we obtain elastic behavior near the critical point. This is consistent with the existence of the inertia-like term. The current model has no intrinsic polarity (direction) and therefore there is marked difference of collision dynamics with that of the linear squirmer model. In the latter, the change of direction is inevitably followed by rotation while the current model could change the direction instantaneously. It has been argued that the competition between self-propulsion and rotational diffusion time plays a relevant role in the collective behavior for the squirmer and Janus particle models (Cates & Tailleur 2015; Matas-Navarro *et al.* 2014). Our study reveals that symmetry-breaking-type swimmer may have another mechanism of competition, possibly between self-propulsion and effect inertia time. This may lead to another phase behavior in the collective behavior of self-propelled particles.

We limited ourselves to the cases where deformation of the drop is not large. We may relax this assumption by changing the parameters and expect intriguing dynamics caused by the coupling between self-propulsion and deformation. We leave this subject for the future study. This work focuses on head-on collision in detail and suggests the importance of concentration-mediated interactions. However, there are other types of collision, namely tangential motion to the centerline between two drops and relative rotation. In these cases, it may be possible that the hydrodynamics play a major role. We think the investigation of these motion is also important in future.

Acknowledgements

The authors are also grateful to Kei-Ichi Ueda and Tanniemola Liverpool for helpful discussions. This work was supported in part by a Grant-in-Aid for Young Scientists (B) (No.26800219 and 15K17737), Grants-in-Aid for Japan Society for Promotion of Science (JSPS) Fellows (Grants Nos. 241799 and 263111), the JSPS Core-to-Core Program "Non-equilibrium dynamics of soft matter and information" and for Scientific Research on Innovative Areas Fluctuation & Structure (No. 26103503).

Appendix A. spherical Bessel function

In this work, we use the spherical Bessel function defined by

$$j_n(x) = \sqrt{\frac{\pi}{2x}} \mathcal{J}_{n+1/2}(x) \quad (\text{A1})$$

where $\mathcal{J}_n(x)$ is the n -th order Bessel function of first kind. The spherical Bessel functions are expressed also in the following ways

$$j_n(x) = (-1)^n x^n \left(\frac{1}{x} \frac{d}{dx} \right)^n \frac{\sin x}{x} \quad (\text{A } 2)$$

The spherical Bessel function satisfies the following relation

$$j'_n(x) = \frac{n}{x} j_n(x) - j_{n+1}(x) \quad (\text{A } 3)$$

where $j'_n(x) = dj_n(x)/dx$. For $n = 0$, it becomes

$$j'_0(x) = -j_1(x). \quad (\text{A } 4)$$

Here we consider the following integral containing three Spherical Bessel functions

$$\begin{aligned} & \int_0^\infty \frac{q^m}{q^2 + \beta^2} j_l(qR_0) j_{l'}(qr_{12}) j_{l''}(qR_0) dq \\ &= (-1)^{l+l'+l''} R_0^{l+l''} r_{12}^{l'} \left(\frac{1}{R_0} \frac{\partial}{\partial R_0} \right)^l \left(\frac{1}{r_{12}} \frac{\partial}{\partial r_{12}} \right)^{l'} \left(\frac{1}{R_0} \frac{\partial}{\partial R_0} \right)^{l''} \int_0^\infty \frac{\sin(qR_0) \sin(qr_{12}) \sin(qR_0)}{R_0^2 r_{12} (q^2 + \beta^2) q^{l+l'+l''+3-m}} dq \end{aligned} \quad (\text{A } 5)$$

Since $l + l' + l''$ is even and m is either $m = 0$ or $m = 2$, the integral does not change under the transformation $q \rightarrow -q$. Now we consider the integral

$$\begin{aligned} I &= \frac{1}{2} \int_{-\infty}^\infty \frac{\sin(qR_0) \sin(qr_{12}) \sin(qR_0)}{(q^2 + \beta^2) q^{l+l'+l''+3-m}} dq \\ &= -\frac{1}{16i} \int_{-\infty}^\infty \frac{(e^{iqR_0} - e^{-iqR_0})^2 (e^{iqr_{12}} - e^{-iqr_{12}})}{(q^2 + \beta^2) q^{l+l'+l''+3-m}} dq. \end{aligned} \quad (\text{A } 6)$$

This integral is calculated from residues $q = 0, \pm\beta$. The main contribution arises from the residue $q = i\beta$ for the integration path passing $+i\infty$ in the positive direction, and from the residue $q = -i\beta$ for the integration path passing $-i\infty$ in the negative direction. For $r_{12} > 2R_0$,

$$\begin{aligned} I &= -\frac{\pi}{8} \left[\lim_{q \rightarrow i\beta} \frac{(e^{iqR_0} - e^{-iqR_0})^2 e^{iqr_{12}}}{(q + i\beta) q^{l+l'+l''+3-m}} - (-1) \lim_{q \rightarrow -i\beta} \frac{(e^{iqR_0} - e^{-iqR_0})^2 e^{-iqr_{12}}}{(q - i\beta) q^{l+l'+l''+3-m}} \right] \\ &= -\frac{\pi}{8} \left[\frac{4 \sinh^2(\beta R_0) e^{-\beta r_{12}}}{2i\beta (i\beta)^{l+l'+l''+3-m}} + \frac{4 \sinh^2(\beta R_0) e^{-\beta r_{12}}}{(-2i\beta)(-i\beta)^{l+l'+l''+3-m}} \right] \\ &= -\frac{\pi}{8} \frac{\sinh^2(\beta R_0) e^{-\beta r_{12}}}{i\beta (i\beta)^{l+l'+l''+3-m}} \end{aligned} \quad (\text{A } 7)$$

Next, we consider the following general integral

$$\begin{aligned} & \int_0^\infty \frac{q^m}{(q^2 + \beta^2)^n} j_l(qR_0) j_{l'}(qr_{12}) j_{l''}(qs) dq \\ &= (-1)^{l+l'+l''} R_0^l r_{12}^{l'} s^{l''} \left(\frac{1}{R_0} \frac{\partial}{\partial R_0} \right)^l \left(\frac{1}{r_{12}} \frac{\partial}{\partial r_{12}} \right)^{l'} \left(\frac{1}{s} \frac{\partial}{\partial s} \right)^{l''} \int_0^\infty \frac{\sin(qR_0) \sin(qr_{12}) \sin(qs)}{R_0 r_{12} s (q^2 + \beta^2)^n q^{l+l'+l''+3-m}} dq. \end{aligned} \quad (\text{A } 8)$$

We calculate the following integral

$$\begin{aligned} I_n &= \frac{1}{2} \int_{-\infty}^{\infty} \frac{\sin(qR_0) \sin(qr_{12}) \sin(qs)}{(q^2 + \beta^2)^n q^{l+l'+3-m}} dq \\ &= -\frac{1}{16i} \int_{-\infty}^{\infty} \frac{(e^{iqR_0} - e^{-iqR_0})(e^{iqr_{12}} - e^{-iqr_{12}})(e^{iqs} - e^{-iqs})}{(q^2 + \beta^2)^n q^{l+l'+3-m}} dq. \end{aligned} \quad (\text{A } 9)$$

For $r_{12} > s > R_0$, we obtain

$$\begin{aligned} I_n &= -\frac{\pi}{8} \left[\lim_{q \rightarrow i\beta} \frac{d^{n-1}}{dq^{n-1}} \frac{(e^{iqR_0} - e^{-iqR_0})(e^{iqs} - e^{-iqs})e^{iqr_{12}}}{(q + i\beta)q^{l+l'+3-m}} \right. \\ &\quad \left. - (-1) \lim_{q \rightarrow -i\beta} \frac{d^{n-1}}{dq^{n-1}} \frac{(e^{iqR_0} - e^{-iqR_0})(e^{iqs} - e^{-iqs})e^{-iqr_{12}}}{(q - i\beta)q^{l+l'+3-m}} \right]. \end{aligned} \quad (\text{A } 10)$$

REFERENCES

- ANDERSON, D. M., MCFADDEN, G. B. & WHEELER, A. A. 1998 Diffuse-interface methods in fluid mechanics. *Annual Review of Fluid Mechanics* **30** (1), 139–165.
- ARFKEN, G.B., WEBER, H.J. & WEBER, H.J. 1968 *Mathematical methods for physicists*. Academic press New York.
- BHAGAVATULA, RAVI, JASNOW, DAVID & OHTA, T. 1997 Nonequilibrium interface equations: An application to thermocapillary motion in binary systems. *Journal of Statistical Physics* **88** (5), 1013–1031.
- BLAKE, JR 1971 Self propulsion due to oscillations on the surface of a cylinder at low reynolds number. *Bulletin of the Australian Mathematical Society* **5** (02), 255–264.
- BODE, M., LIEHR, A.W., SCHENK, C.P. & PURWINS, H.-G. 2002 Interaction of dissipative solitons: particle-like behaviour of localized structures in a three-component reaction-diffusion system. *Physica D* **161** (1-2), 45 – 66.
- CATES, MICHAEL E & TAILLEUR, JULIEN 2015 Motility-induced phase separation. *Annu. Rev. Condens. Matter Phys.* **6** (1), 219–244.
- FEDOSOV, A. I. 1956 Thermocapillary motion (translated by viatcheslav berejnov and konstantin morozov). *Zhurnal Fizicheskoi Khimii (see also arXiv:1303.024)* **30**.
- HETSRONI, GAD & HABER, SHIMON 1970 The flow in and around a droplet or bubble submerged in an unbound arbitrary velocity field. *Rheologica Acta* **9** (4), 488–496.
- HOHENBERG, P. C. & HALPERIN, B. I. 1977 Theory of dynamic critical phenomena. *Rev. Mod. Phys.* **49** (3), 435–479.
- HOWSE, JONATHAN R., JONES, RICHARD A. L., RYAN, ANTHONY J., GOUGH, TIM, VAFABAKHSH, REZA & GOLESTANIAN, RAMIN 2007 Self-motile colloidal particles: From directed propulsion to random walk. *Physical Review Letters* **99** (4), 048102.
- ISHIKAWA, T., SIMMONDS, MP & PEDLEY, TJ 2006 Hydrodynamic interaction of two swimming model micro-organisms. *Journal of Fluid Mechanics* **568**, 119–160.
- ISHIMOTO, KENTA & GAFFNEY, EAMONN A. 2013 Squirmer dynamics near a boundary. *Phys. Rev. E* **88**, 062702.
- IZRI, ZIANE, VAN DER LINDEN, MARJOLEIN N., MICHELIN, SÉBASTIEN & DAUCHOT, OLIVIER 2014 Self-propulsion of pure water droplets by spontaneous marangoni-stress-driven motion. *Phys. Rev. Lett.* **113**, 248302.
- JEFFREY, DJ & ONISHI, Y 1984 Calculation of the resistance and mobility functions for two unequal rigid spheres in low-reynolds-number flow. *Journal of Fluid Mechanics* **139**, 261–290.
- JIANG, HONG-REN, YOSHINAGA, NATSUHIKO & SANO, MASAKI 2010 Active motion of janus particle by self-thermophoresis in defocused laser beam. *Phys. Rev. Lett.* **105**, 268302.
- KAWASAKI, KYOZI & OHTA, TAKAO 1983 Kinetics of fluctuations for systems undergoing phase transitions - interfacial approach. *Physica A* **118** (1-3), 175 – 190.
- KITAHATA, HIROYUKI, YOSHINAGA, NATSUHIKO, NAGAI, KEN H. & SUMINO, YUTAKA 2011

- Spontaneous motion of a droplet coupled with a chemical wave. *Phys. Rev. E* **84** (1), 015101.
- LAUGA, ERIC & POWERS, THOMAS R 2009 The hydrodynamics of swimming microorganisms. *Reports on Progress in Physics* **72** (9), 096601.
- LEVAN, M. DOUGLAS 1981 Motion of a droplet with a newtonian interface. *Journal of Colloid and Interface Science* **83** (1), 11 – 17.
- LI, GAO-JIN & ARDEKANI, AREZOO M. 2014 Hydrodynamic interaction of microswimmers near a wall. *Phys. Rev. E* **90**, 013010.
- LIGHTHILL, M. J. 1952 On the squirming motion of nearly spherical deformable bodies through liquids at very small reynolds numbers. *Communications on Pure and Applied Mathematics* **5** (2), 109–118.
- MATAS-NAVARRO, RICARD, GOLESTANIAN, RAMIN, LIVERPOOL, TANNIEMOLA B. & FIELDING, SUZANNE M. 2014 Hydrodynamic suppression of phase separation in active suspensions. *Phys. Rev. E* **90**, 032304.
- MICHELIN, SASTIEN, LAUGA, ERIC & BARTOLO, DENIS 2013 Spontaneous autophoretic motion of isotropic particles. *Physics of Fluids* **25** (6), 061701.
- NISHIURA, YASUMASA, TERAMOTO, TAKASHI & UEDA, KEI-ICHI 2003 Scattering and separators in dissipative systems. *Phys. Rev. E* **67**, 056210.
- OHTA, TAKAO 2001 Pulse dynamics in a reaction-diffusion system. *Physica D* **151** (1), 61 – 72.
- OHTA, TAKAO, KIYOSE, JUNKO & MIMURA, MASAYASU 1997 Collision of propagating pulses in a reaction-diffusion system. *Journal of the Physical Society of Japan* **66** (5), 1551–1558.
- PAK, ON SHUN & LAUGA, ERIC 2014 *Royal Society of Chemistry Soft Matter Series*, chap. Theoretical models in low-Reynolds-number locomotion.
- PAXTON, W.F., KISTLER, K.C., OLMEDA, C.C., SEN, A., ST.ANGELO, S.K., CAO, Y., MALLOUK, T.E., LAMMERT, P.E. & CRESPI, V.H. 2004 Catalytic nanomotors: Autonomous movement of striped nanorods. *Journal of the American Chemical Society* **126** (41), 13424–13431.
- RYAZANTSEV, YU. S. 1985 Thermocapillary motion of a reacting droplet in a chemically active medium. *Fluid Dynamics* **20**, 491–495, translated from *Izves*iya Akademii Nmuz SSSR, Hekdlanika Zhidkosti i Gaza*, No. 3, pp. 180-183, 1985.
- SCRIVEN, L. E. 1960 Dynamics of a fluid interface equation of motion for newtonian surface fluids. *Chemical Engineering Science* **12** (2), 98 – 108.
- SHAO, DANYING, RAPPEL, WOUTER-JAN & LEVINE, HERBERT 2010 Computational model for cell morphodynamics. *Phys. Rev. Lett.* **105** (10), 108104.
- SPAGNOLIE, SAVERIO E & LAUGA, ERIC 2012 Hydrodynamics of self-propulsion near a boundary: predictions and accuracy of far-field approximations. *Journal of Fluid Mechanics* **700**, 105–147.
- STONE, HOWARD A. & SAMUEL, ARAVINTHAN D. T. 1996 Propulsion of microorganisms by surface distortions. *Phys. Rev. Lett.* **77** (19), 4102–4104.
- THUTUPALLI, SHASHI, SEEMANN, RALF & HERMINGHAUS, STEPHAN 2011 Swarming behavior of simple model squirmers. *New Journal of Physics* **13** (7), 073021.
- TJHUNG, ELSEN, MARENUZZO, DAVIDE & CATES, MICHAEL E. 2012 Spontaneous symmetry breaking in active droplets provides a generic route to motility. *Proceedings of the National Academy of Sciences* **109** (31), 12381–12386.
- TOYOTA, TARO, MARU, NAOTO, HANCZYC, MARTIN M., IKEGAMI, TAKASHI & SUGAWARA, TADASHI 2009 Self-propelled oil droplets consuming "fuel" surfactant. *Journal of the American Chemical Society* **131** (14), 5012–5013.
- USPAL, W. E., POPESCU, M. N., DIETRICH, S. & TASINKEVYCH, M. 2015 Self-propulsion of a catalytically active particle near a planar wall: from reflection to sliding and hovering. *Soft Matter* **11**, 434–438.
- WATSON, G.N. 1922 *A treatise on the theory of Bessel functions*. Cambridge Univ Pr.
- YABUNAKA, S., OHTA, T. & YOSHINAGA, N. 2012 Self-propelled motion of a fluid droplet under chemical reaction. *The Journal of Chemical Physics* **136** (7), 074904.
- YAM, PATRICIA T., WILSON, CYRUS A., JI, LIN, HEBERT, BENEDICT, BARNHART, ERIN L., DYE, NATALIE A., WISEMAN, PAUL W., DANUSER, GAUDENZ & THERIOT, JULIE A. 2007 Actin myosin network reorganization breaks symmetry at the cell rear to spontaneously initiate polarized cell motility. *J. Cell Biol.* **178** (7), 1207–1221.

- YOSHINAGA, NATSUHIKO 2014 Spontaneous motion and deformation of a self-propelled droplet. *Phys. Rev. E* **89**, 012913.
- YOSHINAGA, NATSUHIKO, NAGAI, KEN H., SUMINO, YUTAKA & KITAHATA, HIROYUKI 2012 Drift instability in the motion of a fluid droplet with a chemically reactive surface driven by marangoni flow. *Phys. Rev. E* **86**, 016108.
- YOUNG, N. O., GOLDSTEIN, J. S. & BLOCK, M. J. 1959 The motion of bubbles in a vertical temperature gradient. *Journal of Fluid Mechanics* **6** (03), 350–356.
- ZIEBERT, FALKO, SWAMINATHAN, SUMANTH & ARANSON, IGOR S. 2012 Model for self-polarization and motility of keratocyte fragments. *Journal of The Royal Society Interface* **9** (70), 1084–1092.